Real-time Detection of Low-frequency Oscillations in Traction Power Supply Systems Based on Optimized Atomic Decomposition

Jun Zhu, Zhaoyang Li, Yu Xie, and Haitao Hu

***Abstract*—Low-frequency oscillations (LFOs) in traction power supply systems (TPSSs) frequently arise when multiple electric trains simultaneously raise their pantographs under the same power supply arm. This phenomenon is characterized by low-frequency fluctuations (2–8 Hz) in the envelope waveforms of traction network voltage and current. It can lead to operational issues such as insufficient current acquisition and difficulties in depot entry or exit, thereby adversely affecting railway operations. Given the time-varying nature of LFOs, timely and accurate detection is critical for implementing effective mitigation strategies, with faster detection enabling improved outcomes. This paper proposes a real-time detection algorithm for LFOs in AC traction networks that integrates signal preprocessing, spectral analysis, and parameter optimization. First, the voltage signal is processed using a low-pass filter to suppress high-frequency noise. Then, a fast Fourier transform (FFT)-based spectral estimation method is applied to extract frequency-domain features. Oscillation parameter identification is triggered when the identified signal amplitude exceeds predefined thresholds in the 42–48 Hz and 52–58 Hz bands. Subsequently, during the identification stage, an LFO atom dictionary is constructed based on the FFT pre-analysis results. Finally, the matching pursuit algorithm is employed to achieve fast and accurate extraction of LFO parameters. The proposed method is validated using both simulated and real-world measurement data. Experimental results confirm its effectiveness in detecting LFOs under noisy conditions, demonstrating high accuracy and computational efficiency. The approach provides valuable insights for the threshold selection of protection devices, thereby enhancing the stability and reliability of TPSSs.**

***Index Terms*—Traction power supply system, low-frequency voltage oscillation, atomic decomposition, signal processing.**

I. Introduction

In recent years, with the increasing deployment of AC-DC-AC drive electric trains, low-frequency oscillation (LFO) events have been reported globally across various types of traction power supply systems (TPSSs) [1], [2]. When electric trains start operating—for instance, when pantographs are raised—impedance mismatches between onboard converters and the TPSS can induce low-frequency voltage oscillations. These oscillations, arising from train-network coupling, may lead to serious operational disturbances such as traction lock, which not only reduce locomotive performance but also threaten railway safety [3]–[5].

According to published reports, the first recorded case of LFO in China occurred in December 2007 at the Hudong locomotive depot on the Daqin railway [4], where several HXD1 electric trains were powered up simultaneously, triggering traction network voltage oscillations around 3 Hz. To further investigate the LFO phenomenon, field tests were conducted at a railway substation in December 2021. As shown in Fig. 1, the measured oscillation frequency was approximately 3.8 Hz, and the RMS voltage during the oscillation period exceeded 36 kV.

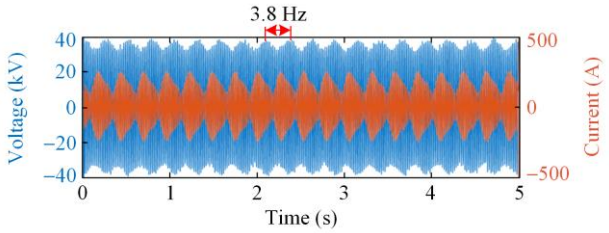

Fig. 1. Field test LFO waveform data.

Such oscillations can result in system protection malfunction and increase unscheduled downtime of electric trains. Subsequent incidents of LFOs have been reported in different regions across China with various

Received: November 11, 2024
Accepted: June 28, 2025
Published Online: November 1, 2025
Jun Zhu, Zhaoyang Li (corresponding author), Yu Xie, and Haitao Hu are with the School of Electrical Engineering, Southwest Jiaotong University, Chengdu 610031, China (e-mail: zhujun@my.swjtu.edu.cn; lzy@swjtu.edu.cn; 2024200439@my.swjtu.edu.cn; hht@swjtu.edu.cn).
DOI: 10.23919/PCMP.2024.000415

oscillation frequencies. Table I presents a summary of notable LFO cases [6]–[8].

TABLE I
SOME CASES OF LFOS IN TPSSS

No.	Types of trains	Frequency of oscillation (Hz)	Date	Testing position
1	HXD1	2–4	2007.12	Hudong depot
2	CRH1	5	2008.01	Shanghai Nanxiang train depot
3	CRH5	5	2010.09	Qingdao train depot
4	HXD2B	2	2015.11	Xuzhoubei traction substation
5	HXD3B	6–7	2018.05	Shanhaiguan railway junction

These LFO incidents have significantly impacted railway operations. The resulting voltage fluctuations in the traction networks can lead to power loss and disruptions in train scheduling. In addition, LFOs can cause excessive voltage and current oscillations, potentially leading to insulation damage, capacitor bank burnout, and lightning arrester failure. Because LFOs evolve over time, timely detection is crucial to enable appropriate suppression. Accordingly, developing a real-time LFO detection method is vital for railway management to intervene effectively, thereby enhancing both safety and operational efficiency [9], [10].

There are many methods for detecting LFOs, such as the fast Fourier transform (FFT) [11], wavelet transform (WT) [12], Prony algorithm [13], Hilbert-Huang transform (HHT) [14], and atomic decomposition (AD) [15]. The advantages and disadvantages of these methods are compared in Table II.

TABLE II
DIFFERENT METHODS FOR IDENTIFYING LFOS

Method	Advantages	Disadvantages	Application scenarios
FFT [11]	1) Simple to implement, fast computation 2) Suitable for periodic signals	1) Frequency resolution is limited by the window size 2) Only suitable for stationary signals	Suitable for cases with stable frequencies and low resolution requirements
WT [12]	1) Able to analyze signals in both the time and frequency domains 2) Suitable for nonstationary signals	1) Depends on the subjective choice of the mother wavelet 2) High computational complexity	Suitable for signals with large time-frequency variations, especially transient analysis
Prony algorithm [13]	1) Efficient in analyzing decaying modes 2) Capable of identifying multiple frequency components	1) Sensitive to noise, leading to inaccurate parameter estimation 2) High computational complexity	Suitable for frequency estimation of signals with exponential decay
HHT [14]	1) Suitable for nonlinear, nonstationary signals 2) Provides high time-frequency resolution	1) High computational complexity 2) Relies on empirical mode decomposition (EMD), prone to overfitting	Suitable for analyzing nonlinear, nonstationary signals with large frequency variations
AD [15]	1) Flexible in handling complex signals 2) Suitable for sparse decomposition of time-varying signals	1) Depends on the design of the atomic dictionary, results may not be unique 2) High computational complexity	Suitable for precise analysis of sparse signals, especially for LFO detection.

The accuracy of the frequency identified by the FFT algorithm is limited by the data window, and the frequency resolution is calculated as:

$$\Delta f = \frac{f_S}{N} \tag{1}$$

where Δf is the frequency resolution; f_S is the sampling frequency; and N is number of the sampling point. According to (1), for an oscillation frequency detection accuracy to be at least 0.1 Hz, a 10 s data window is needed, making real-time detection challenging [11]. WT offers multiresolution analysis but relies heavily on the subjective selection of wavelet basis functions, making it complex to implement [12]. The Prony algorithm excels in analyzing signals with exponential decay, but it is highly sensitive to noise, which affects its parameter estimation accuracy [13]. HHT, on the other hand, is powerful for processing nonstationary signals but suffers from high computational complexity, thereby limiting its real-time application [14].

In addition, in terms of real-time detection algorithms, convolutional neural network methods have been used to detect abnormal electrical disturbances in TPSSs, including LFOs [16], achieving preliminary automation in identifying abnormal electrical phenomena on electrified railways. Some studies have also used the XGBoost ensemble learning algorithm to classify electrical anomalies in TPSSs [17]. Reference [18] improves total least squares-estimating signal parameter via rotational invariance techniques (TLS-ESPRIT) algorithm to accurately obtain the key modal parameters of disturbances, and defines the disturbance severity assessment index based on the characteristics and the key modal parameters of each disturbance. This method can effectively and quickly identify the type of abnormal disturbance in the traction power supply system and evaluate its severity.

Recently, AD algorithms have emerged as a prominent approach in signal processing, attracting significant interest from researchers and practitioners [15]. This methodology is rooted in the concept of decomposing signals through an overcomplete atom library, as

proposed in [19]. Performing AD on signals substantially increases both the simplicity and flexibility of signal representation. This technology plays a crucial role in various applications, such as signal modelling, compression, and feature extraction. In recent years, AD methods have been successfully applied to power system signal analysis. In [20], the time-frequency atomic decomposition algorithm is utilized to analyze inter-harmonics in power systems. Building on this, reference [21] introduces a discrete Gabor atom library combined with traditional matching and tracking algorithms. In [22] and [23], a discrete correlated atom library is specifically developed for disturbance signals in power systems, which has significantly lower computational complexity than that of the approach in [24]. Furthermore, particle swarm optimization (PSO) algorithms are employed in [25] and [26] to improve the matching and tracking process for inter-harmonic detection and analysis.

Several studies have focused on applying AD methods to analyze LFOs in power systems. For example, reference [27] proposes a direct attenuated sinusoidal atomic library decomposition method that integrates chaos theory with pseudo-Newton optimization techniques to address challenges related to discretization and optimization efficiency in six-dimensional space. In [28], an innovative approach is presented for identifying LFO modes by transforming the selection of modal atoms into an optimization problem, which is then solved via PSO algorithms. Each modal atom corresponds to an oscillation mode, thereby facilitating the identification of LFO modal parameters. LFOs in power systems are generally power oscillations, with low oscillation frequencies, typically in the range of 0.1–2.5 Hz, and are stable. However, LFOs in TPSSs differ fundamentally from those in conventional power systems in both generation mechanisms and signal characteristics, as the oscillation frequency in TPSSs varies with trains' operating state. Consequently, existing methods are unable to meet the requirements of real-time LFO detection in TPSSs.

This study proposes a real-time detection algorithm for LFO phenomena in AC traction networks, which integrates signal preprocessing, spectral analysis, and parameter optimization. Initially, the voltage signal undergoes low-pass filtering to eliminate high-frequency interferences, followed by FFT spectral estimation to quantify frequency-domain characteristics. Upon detection of amplitude thresholds exceeding preset values (42–48 Hz and 52–58 Hz frequency bands), the system activates parameter identification through a dynamically optimized atomic library constructed from FFT spectral data. Simulation studies and measured data demonstrate that the proposed method significantly reduces the optimization range and computational complexity of the conventional matching pursuit (MP) algorithm, while exhibiting strong noise robustness and generalization capability.

The structure of the rest of the paper is as follows. Section II describes LFO detection method based on optimized AD. In Section III, various cases are examined to demonstrate the effectiveness of the proposed method. Finally, conclusions are drawn in Section IV.

II. LFO Detection Method Based on Optimized Atomic Decomposition

A. Data Preprocessing

Frequency is one of the important evaluation indicators of LFO phenomenon in TPSS. If the disturbance frequency parameter to be extracted can be quickly estimated in each iteration of the matching pursuit algorithm, the search range of subsequent parameters can be reduced, thereby accelerating the overall search process. FFT is an efficient method for obtaining signal spectrum. By exploiting the periodicity and symmetry of discrete Fourier transform (DFT), FFT reduces the computational complexity of DFT from $O(N^2)$ to $O(N \log N)$, greatly improving the computational efficiency.

As shown in (1), when FFT is directly applied to analyze LFO signals, the frequency resolution is inherently limited. Achieving higher frequency resolution requires a longer data window, which in turn necessitates data acquisition devices with large memory capacity and long-duration continuous storage. However, since the frequency components of power quality disturbances are typically discrete and limited in number, a more efficient strategy can be adopted. Specifically, FFT is first used to approximate the frequency distribution of the signal. Based on this pre-analysis, frequency atoms are re-discretized around the identified spectral peaks, after which the MP algorithm is applied for targeted parameter extraction.

It should be noted that applying FFT to non-stationary or asynchronously sampled signals may result in spectral leakage and picket-fence effects, leading to inaccurate estimation of amplitude and phase parameters. Therefore, in this study, only the frequency parameter range is optimized based on FFT results.

Since LFO disturbance components are primarily concentrated within the 42–58 Hz range, components outside this band not only increase computational burden but also interfere with the subsequent MP process, thereby affecting accuracy. Consequently, it is necessary to remove high-order harmonics prior to FFT-based frequency estimation. In this work, a Butterworth-based zero-phase low-pass filter [29] is used to suppress harmonic components above 100 Hz, thereby preventing high-frequency content from distorting the MP results. Taking the simulated signal described by Eq. (15) in Section III.A.2) as an example, Fig. 2 compares the results before and after filtering.

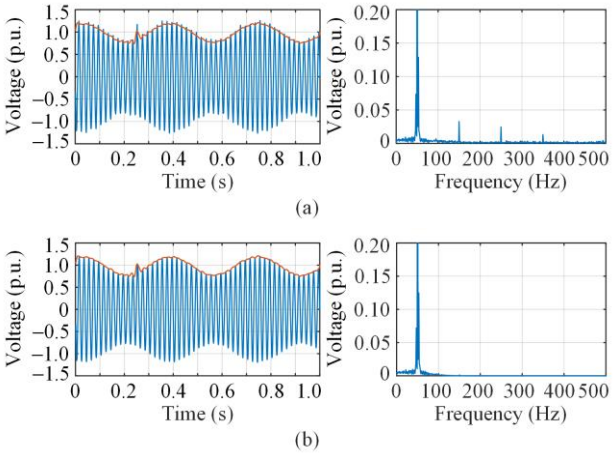

Fig. 2. Comparison of Butterworth low-pass filtering effects before and after. (a) Original signal and its spectrum. (b) Filtered signal and its spectrum.

As shown in Fig. 2, the proposed method effectively preserves the low-frequency components of the signal while attenuating high-frequency components above 100 Hz. This suppression minimizes interference in the subsequent LFO component extraction process, thereby enhancing the accuracy of signal decomposition.

B. LFO Overcomplete Atom Library

In general, the sinusoidal attenuation model of the power quality disturbance signal is as follow:

$$g(t)=A\cos(2\pi ft+\varphi)\mathrm{e}^{-\alpha(t-t_s)}\left[u(t-t_s)-u(t-t_e)\right] \quad (2)$$

where f is the frequency; φ is the phase position; A is the amplitude of the damped sinusoidal quantity; t_s is the start time of disturbance; t_e is the end time of disturbance; and $u(\cdot)$ is the unit step function. As shown in (2), the model has 6 parameters which are optimized using sparse signal decomposition.

According to [27], LFO signals observed in TPSSs are typically caused by interharmonic components that appear near the fundamental frequency. Based on extensive field tests, it has been observed that these interharmonics remain relatively stable, typically persisting for durations ranging from several tens of seconds to several minutes. Within this time window, LFO signals can be reasonably approximated as a steady-state disturbance.

Therefore, the LFO atom dictionary constructed in this study does not account for the start and end times of individual oscillatory components. This assumption reduces the number of parameters required for modeling, thereby decreasing the overall computational burden. When an LFO event occurs in a TPSS, the instantaneous envelopes of the voltage and current in the traction network exhibit low-frequency (0.1–10 Hz) fluctuations with nearly constant amplitude and frequency, containing a significant number of interharmonic components denoted as $f_1 \pm f_{osc}$. The time domain waveform expression of the voltage is:

$$\begin{aligned} u(t)=&U_1\cos\left(2\pi f_1 t+\delta_1\right)+\\ &U_{1+}\cos\left[2\pi\left(f_1+f_{osc}\right)t+\delta_{1+}\right]+\\ &U_{1-}\cos\left[2\pi\left(f_1-f_{osc}\right)t+\delta_{1-}\right] \end{aligned} \quad (3)$$

where U_1, f_1, δ_1 are the amplitude, frequency and phase of the fundamental component, respectively; f_{osc} is the oscillation frequency; U_{1+} and δ_{1+} are the amplitude and phase of the first oscillation component respectively; U_{1-} and δ_{1-} are the amplitude and phase of the second oscillation component, respectively. Equation (5) does not account for the integer harmonics caused by pulse width modulation (PWM) control, as these do not affect the extraction of LFO components and are out the scope of this paper.

The analysis of measured LFO data in TPSS shows that all typical LFO waveforms can be expressed by the unified time domain waveform expression described by (3). It shows that following the occurrence of LFO, in addition to the power frequency fundamental component, there are also inter-harmonic components on the left and right sides of the fundamental frequency. This is the primary reason why the instantaneous voltage envelope shows low-frequency fluctuations. The oscillating voltage and current waveforms may either appear in phase or in opposite phase, which constitutes an important feature that distinguishes LFO from other disturbance signals.

Further analysis shows that the amplitudes of components f_1+f_{osc} and f_1-f_{osc} are usually differ significantly. Based on this, an LFO atomic library for TPSS can be constructed as:

$$g(t)=A_2\cos\left(2\pi f_2 t+\varphi_2\right) \quad (4)$$

where $\gamma_2=\left[f_2,\ \varphi_2\right]$ is the parameter set of the LFO atom library; $f_2=f_1\pm f_{osc}$ is the frequency of the LFO atom library; φ_2 is the phase of the LFO atom library; and A_2 is the coefficient that makes $\|g(t)\|=1$.

By discretizing the parameters in (4), an overcomplete atom library that meets the characteristics of the LFO waveform can be obtained. The frequency parameters of the LFO atom library can be set to:

$$\left(f_{peak}-0.5\right)\ \mathrm{Hz}\leqslant f_2\leqslant\left(f_{peak}+0.5\right)\ \mathrm{Hz} \quad (5)$$

where f_{peak} is the integer frequency estimated by the FFT spectrum analysis, and is within the range of:

$$42\ \mathrm{Hz}\leqslant f_{peak}\leqslant 58\ \mathrm{Hz} \quad (6)$$

The frequency resolution is 0.01 Hz, and the phase parameters can be discretized to:

$$0\leqslant\varphi_2<2\pi \quad (7)$$

The phase resolution is 0.01 rad. After the above discretization processing, the total number of atoms in the LFO atomic library is 1601×628, which can cover the LFO components of all frequency bands in the signal.

When the voltage signal is analyzed by the AD algorithm, it can be obtained by searching for the frequency, phase and amplitude parameters of the best-matching atoms in the overcomplete correlation atom library via the MP algorithm. Because the AD algorithm does not involve the correction analysis of spectral lines in the frequency domain, there is no need to consider the influence of spectral interference. Theoretically, as long as the atomic library constructed via atomic decomposition is overcomplete, it has sufficient frequency resolution.

C. MP Algorithm

Sparse signal decomposition typically uses a greedy adaptive decomposition strategy—the MP algorithm. As the primary method for sparse decomposition, MP is a greedy iterative algorithm. In each iteration, the algorithm scans the atomic dictionary to identify the atom most correlated with the analysis signal, then extracts its energy from the signal to generate a new residual. The matching process can be controlled either by setting the number of iterations or by limiting the residual energy.

Define the overcomplete atomic library as $D=(g_\gamma)_{\gamma\in\Gamma}$, where γ is the atomic parameter group and Γ is the set of atomic parameter groups. All the atoms are normalized so that $\|g_\gamma\|=1$. In each iteration, the MP seeks an atom $g_{\gamma(m)}\in D$ that has the greatest inner product with the current residual signal r_{f}^{m-1} (m is the number of iterations). After each iteration, the atom $g_{\gamma(m)}$ is extracted from the residual signal to form a new residual signal.

Assuming that the signal to be analyzed is $x=r^0$, in the mth iteration decomposition, the atom $g_{\gamma(m-1)}$ in the library that best matches the residual signal and satisfies the following equation is discovered:

$$\left|\left\langle r^{m-1},g_{\gamma(m-1)}\right\rangle\right|=\max_{\gamma\in\Gamma}\left|\left\langle r^{m-1},g_\gamma\right\rangle\right| \tag{8}$$

The residual signal r^{m-1} is decomposed into a new residual component r^m and other components on the basis of the best-matched atom $g_{\gamma(m-1)}$, as:

$$r^{m-1}=\left\langle r^{m-1},g_{\gamma(m-1)}\right\rangle g_{\gamma(m-1)}+r^m \tag{9}$$

For each decomposed residual component, iterative decomposition is repeated according to (8) and (9).

After n iterations, the signal x can be represented as:

$$x=\sum_{m=0}^{n-1}\left\langle r^m,g_{\gamma(m)}\right\rangle g_{\gamma(m)}+r^n \tag{10}$$

For a finite-length signal x, as n increasing indefinitely, $\|r^n\|$ decays exponentially to 0, and the signal x can be represented as:

$$x=\sum_{m=0}^{n-1}\left\langle r^m,g_{\gamma(m)}\right\rangle g_{\gamma(m)} \tag{11}$$

That is, x can be represented as a linear combination of n atoms. Figure 3 shows a graphical representation of the decomposition process of the MP algorithm.

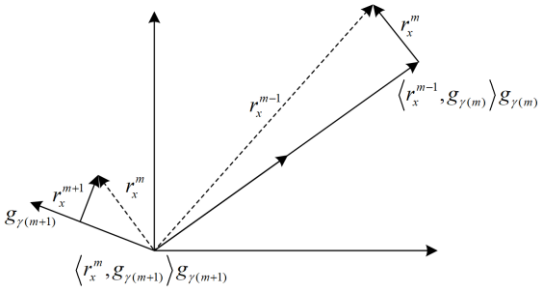

Fig. 3. Signal decomposition process of the MP algorithm.

Equations (8)–(11) show that all atoms in the overcomplete atom library must perform inner product operations with the analyzed signal each time, requiring multiple decompositions. This leads to large amount of calculations, thereby limiting the practicality of the AD algorithm. Therefore, the MP algorithm is often used in combination with other optimization algorithms to improve the calculation speed.

D. LFO Detection Method Based on Optimized AD

As discussed in Section II.B, the interharmonic components near the fundamental frequency are the main cause of LFOs in traction networks. Based on this feature of the voltage signal and combined with the AD algorithm, this paper designs a fast detection method for LFOs in the voltage of an electrified railway traction network. The flowchart of this method is shown in Fig. 4.

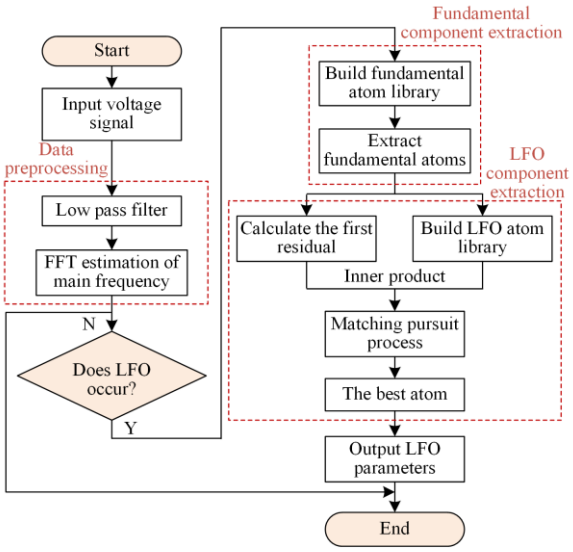

Fig. 4. The flowchart of LFO detection based on optimized AD.

The traction network voltage signal can be acquired either from the voltage sensor on the locomotive's on-board transformer or from the bus voltage transformer at the traction substation. The specific steps are as follows.

Step 1: Data preprocessing. The input voltage signal is first processed using a low-pass filter to suppress high-order harmonics and other unwanted components. The filtered signal is subsequently analyzed using FFT to obtain its spectral distribution. If a significant spectral component is found in the low-frequency band (42–58 Hz) with an amplitude exceeding 0.01 times a predefined reference value, the LFO detection module is activated. Otherwise, the signal is considered free of LFO. The reference value depends on the measurement location, i.e., 27.5 kV for the bus voltage at the substation outlet and 25 kV at the locomotive pantograph.

Step 2: Fundamental component extraction. A fundamental frequency atom dictionary is constructed. A first-stage MP is applied to extract the dominant fundamental component from the signal, followed by computation of the first residual signal.

Step 3: LFO components extraction. Based on the dominant frequency point identified in the residual signal from Step 2, the frequency parameter is discretized over a narrow range (±1 Hz) centered around the dominant frequency, according to Eq. (6). Simultaneously, the phase parameter of the LFO atom is discretized to construct an LFO atom dictionary. The dictionary is then matched with the residual signal to extract the corresponding LFO components. The frequency and phase parameters of the matched atom represent the identified LFO characteristics.

Step 4: Similarity evaluation. In each MP iteration, the extracted atoms contain detailed parameter information about the disturbance signal. These atoms are subsequently used to reconstruct the original disturbance signal, enabling accurate characterization of its low-frequency content. The similarity C_m is used to measure its reconstruction performance, which is defined as:

$$C_m = \frac{\langle y, y_m \rangle}{\|y\| \times \|y_m\|} \tag{12}$$

where y is the original signal and y_m is the reconstructed signal.

E. Computational Complexity Analysis

In the AD process, the algorithm searches for the best-matching atom from a redundant dictionary. If the dictionary contained atoms at all possible frequencies (e.g., spanning a wide range from 0 Hz to several kHz with fine resolution), the computational burden would be extremely high.

Suppose there are N samples in the signal and M atoms in the dictionary, each iteration requires $\mathrm{O}(NM)$, operations (correlation between the signal and all atoms). The total complexity for K iterations is $\mathrm{O}(KNM)$. When conducting MP with FFT preprocessing, the complexity of FFT is $\mathrm{O}(N \log N)$, the complexity of frequency selection is $\mathrm{O}(N)$ (finding some dominant peaks), and the reduced dictionary size is M' $(M' << M)$. Therefore, the MP complexity per iteration is $\mathrm{O}(NM')$, and the total complexity is $\mathrm{O}(N \log N) + \mathrm{O}(KNM')$. Since $M' << M$, for a certain N, the computational burden is greatly reduced.

Overall, FFT-based preprocessing effectively narrows the search space for the matching pursuit algorithm, thereby reducing computational complexity. Rather than searching the entire atom dictionary, the algorithm only needs to focus on a limited number of frequency bands centered around key spectral components. Moreover, this study focuses on LFO detection using a single-channel traction network voltage signal, which further simplifies the algorithm compared to approaches based on multi-sensor or multi-channel monitoring systems.

III. Case Study

In actual TPSSs, the power quality disturbance signals are often the result of the combined action of multiple disturbances, such as LFO, harmonics, voltage swell/sag/interruption, pulse interference and noise. In order to verify the generalization ability of the algorithm in this paper, this section will verify the effectiveness of the algorithm by constructing composite signals of different disturbance types through simulation and field measured data of traction substations and different types of trains.

A. Simulated Data Verification

In the MATLAB 2024 environment, the base frequency of the simulated signal is set to 50 Hz, the sampling frequency is 1 kHz, and the detection time window is 1 s. The signal amplitude is normalized to per-unit (p.u.) values, and Gaussian white noise is added to simulate real-world operating conditions. The LFO detection threshold is defined as 0.01 times the reference voltage amplitude.

It is worth noting that the time window duration is carefully determined based on two key criteria:

1) Lowest frequency constraint. To capture at least one full cycle of the lowest LFO frequency (2 Hz), a minimum window length of 0.5 s is required;

2) Noise robustness. Empirical tests show that excessively short time windows (e.g., less than 0.5 s) exhibit increased sensitivity to transient disturbances and Gaussian noise.

Therefore, a 1 s window is selected, which not only satisfies frequency resolution requirements but also significantly reduces the size of the atom dictionary. Furthermore, the sampling frequency of 1 kHz satisfies the Nyquist-Shannon criterion with a safety factor of 2.5, corresponding to a maximum LFO frequency of 8 Hz, i.e., $8 \times 2.5 = 20$ Hz.

These parameter settings achieve a balance between computational efficiency and detection accuracy, ensuring robustness in practical applications while addressing hardware and resource constraints.

1) Simulation Case 1

The composite disturbance signal includes voltage sag component (duration from 0.030 s to 0.352 s), LFO component, 5th, 7th, and 9th harmonic components, and Gaussian white noise with a signal-to-noise ratio (SNR) of 30 dB, i.e., $n(t)$. Its mathematical expression is as follows:

$$\begin{aligned} u(t) = {} & 1.012\cos(2\pi \times 50t + 1.44) + \\ & A_{\mathrm{l}} \cos(2\pi \times 50t + 1.57) + \\ & 0.105\cos(2\pi \times 57.20t + 0.38) + \\ & 0.042\cos(2\pi \times 250t + 0.56) + \\ & 0.036\cos(2\pi \times 350t + 1.82) + \\ & 0.024\cos(2\pi \times 450t + 2.01) + n(t) \end{aligned} \tag{13}$$

where

$$A_{\mathrm{l}} = \begin{cases} 0.95, & 0.030 \text{ s} \leqslant t \leqslant 0.352 \text{ s} \\ 0, & \text{others} \end{cases} \tag{14}$$

The signal time domain waveform and spectrum analysis results of simulation case 1 are shown in Fig. 5. It can be seen that the envelope of the signal fluctuates at about 7 Hz, which is consistent with the characteristics of the LFO data measured on site.

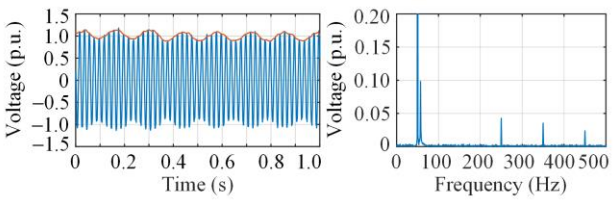

Fig. 5. The signal time domain waveform and spectrum analysis results of simulation case 1.

The filtered signal is subjected to the first matching pursuit using the fundamental wave atom library and the residual is calculated. The obtained fundamental component is shown in Fig. 6.

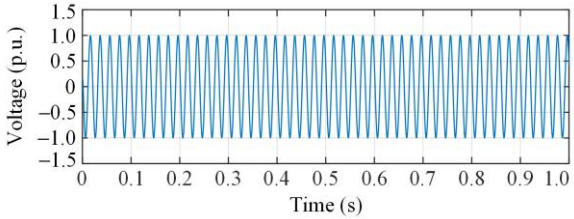

Fig. 6. The fundamental component of simulation case 1.

According to the FFT results, the dominant frequency of the low-frequency band is 57 Hz. The frequency parameters are discretized locally near this frequency point to construct an LFO atom library. The matching pursuit calculation is performed with the first residual signal to obtain the LFO atom and the final residual signal, as shown in Figs. 7 and 8.

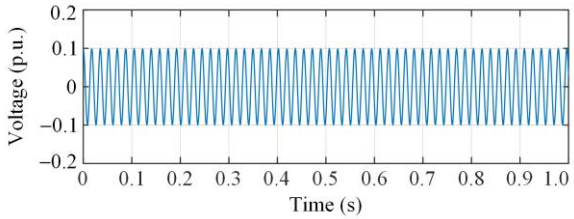

Fig. 7. The LFO component of simulation case 1.

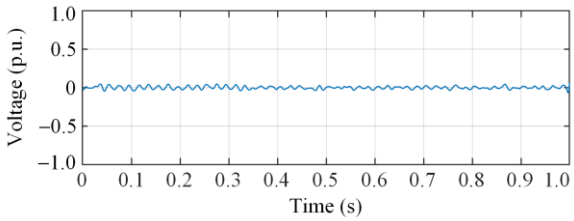

Fig. 8. The final residual signal of simulation case 1.

The signal is reconstructed according to the results of atomic decomposition at each layer. The comparison between the reconstructed signal and the original signal is shown in Fig. 9. According to Eq. (12), the waveform similarity between the reconstructed signal and the original signal is 99.74%. This proves that the proposed algorithm can truly reflect the characteristics of the original signal.

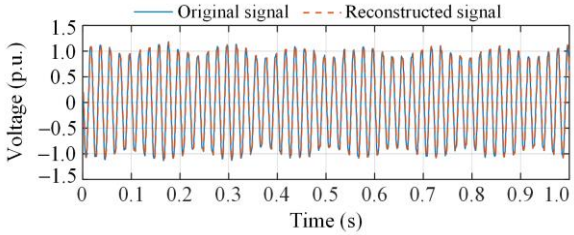

Fig. 9. The comparison between the reconstructed signal and the original signal of simulation case 1.

Under the conditions of Gaussian white noise with different SNR (10 dB, 20 dB, and 30 dB), the matching parameters of each component in the signal decomposition process are shown in Table III.

TABLE III
MATCHING PARAMETERS OF CASE 1

SNR (dB)	Components	Calculated frequency value (Hz)	Calculated phase value (rad)	Calculated amplitude (p.u.)	Similarity (%)
30	Fundamental	49.99	1.47	0.9982	99.74
	LFO	57.20	0.35	0.0966	
20	Fundamental	49.99	1.47	0.9998	99.37
	LFO	57.20	0.35	0.0978	
10	Fundamental	49.99	1.47	1.0023	95.09
	LFO	57.20	0.35	0.1161	

2) Simulation Case 2

The simulation signal of case 2 contains a voltage pulse signal $\delta(t)$ occurring at 0.25 s, two LFO components, 3rd, 5th, and 7th harmonic components, and a Gaussian white noise with an SNR of 30 dB, i.e., $n(t)$. The expression of the signal is as follows:

$$\begin{aligned} u(t) = {} & 1.005\cos(2\pi\times 50.02t + 1.89) + \\ & 0.15\delta(t-0.25) + \\ & 0.144\cos(2\pi\times 53.8t + 1.56) + \\ & 0.075\cos(2\pi\times 46.2t + 2.74) + \\ & 0.032\cos(2\pi\times 150t + 1.89) + \\ & 0.025\cos(2\pi\times 250t + 0.45) + \\ & 0.014\cos(2\pi\times 350t + 2.16) + n(t) \end{aligned} \tag{15}$$

The signal time domain waveform and spectrum analysis results of simulation case 2 are shown in Fig. 10. It can be seen that the envelope of the signal fluctuates at about 4 Hz, and the voltage changes suddenly at 0.25 s, which is consistent with the characteristics of the field measured data.

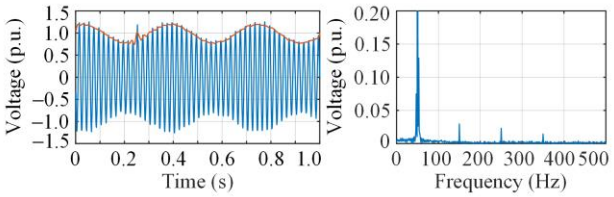

Fig. 10. The signal time domain waveform and spectrum analysis results of simulation case 2.

The filtered signal is subjected to the first matching pursuit using the fundamental wave atom library and the residual is calculated. The obtained fundamental component is shown in Fig. 11.

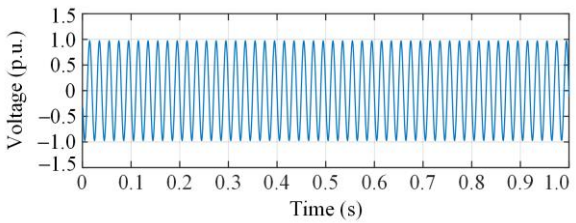

Fig. 11. The fundamental component of simulation case 2.

According to the FFT results, the dominant frequency of the low-frequency band is 54 Hz and 46 Hz. The frequency parameters are discretized locally near these two frequency points to construct LFO atom libraries. The matching pursuit calculation is performed with the first residual signal to obtain the two LFO atoms unitas shown in Figs. 12 and 13.

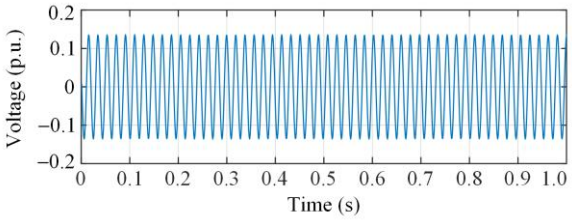

Fig. 12. The first LFO component of simulation case 2.

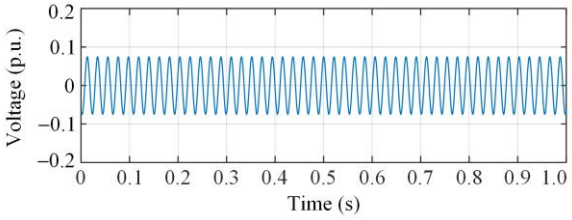

Fig. 13. The second LFO component of simulation case 2.

The final residual signal is illustrated in Fig. 14. As shown, an abrupt change occurs at 0.25 s. This phenomenon arises because the proposed method does not include an atomic dictionary specifically designed for pulse-type disturbances, and the LFO atom library is capable of extracting only signal components that resemble its predefined oscillatory characteristics. If a disturbance component cannot be linearly represented by the atoms in the constructed dictionary, it will remain in the residual signal. This outcome highlights a fundamental principle in atom dictionary design: an overcomplete dictionary must be tailored to capture a specific type of characteristic disturbance.

The signal is reconstructed according to the results of atomic decomposition at each layer. The comparison between the reconstructed signal and the original signal is shown in the Fig. 15. According to Eq. (12), the waveform similarity between the reconstructed signal and the original signal is 99.76%, demonstrating that the proposed algorithm in this paper can truly reflect the characteristics of the original signal.

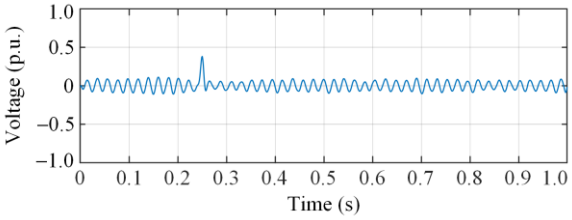

Fig. 14. The final residual signal of simulation case 2.

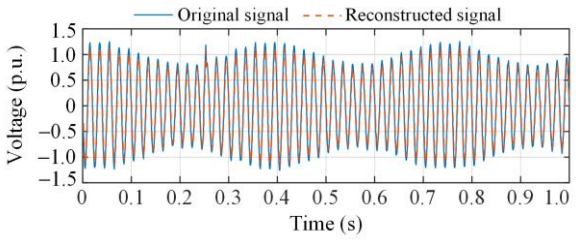

Fig. 15. The comparison between the reconstructed signal and the original signal of simulation case 2.

Under the conditions of Gaussian white noise with different SNR (10 dB, 20 dB, and 30 dB), the matching parameters of each component in the signal decomposition process are shown in Table IV.

TABLE IV
MATCHING PARAMETERS OF CASE 2

SNR (dB)	Calculated frequency value (Hz)	Calculated phase value (rad)	Calculated amplitude (p.u.)	Similarity (%)
30	50.01	1.93	0.9784	99.76
	53.80	1.56	0.1384	
	46.20	2.72	0.0777	
20	50.01	1.93	0.9826	99.31
	53.80	1.56	0.1393	
	46.20	2.78	0.0832	
10	50.02	1.90	0.9848	95.52
	53.85	1.68	0.1360	
	46.12	2.59	0.0701	

In conclusion, the proposed algorithm accurately identifies the frequency, phase, and amplitude parameters of LFO disturbances under various SNR conditions. In terms of signal reconstruction performance, even under severe noise interference with an SNR as low as 10 dB, the algorithm maintains a waveform similarity exceeding 95%. These results demonstrate the algorithm's strong robustness against Gaussian white noise and confirm its effectiveness in practical noisy environments.

B. Comparison Between Optimized AD and Other Existing Methods

This study investigates various detection methods for LFOs and enhances both the detection accuracy and computational efficiency of the proposed algorithm. The ultimate goal is to enable real-time monitoring of LFOs in TPSSs. Once an LFO event is detected, the monitoring system rapidly identifies its characteristic parameters and analyzes the oscillation mechanism by tracking variations in features such as amplitude and frequency. Based on this analysis, appropriate control strategies can be formulated, e.g., either manually or automatically isolating and eliminating the source of the oscillation. In this way, a closed-loop process is established that spans from oscillation occurrence, to detection, and to active suppression, allowing LFOs to be identified and controlled at an early stage. This minimizes potential disruptions and ensures the safe and stable operation of the TPSS.

In the following section, the advantages and limitations of the proposed algorithm will be discussed in terms of detection accuracy, computational speed, and noise robustness. The simulation is conducted on a system configured with an Intel® Core™ i5-8400 CPU@2.80 GHz, 16.0 GB RAM, running a 64-bit Windows 11 operating system and MATLAB R2024b.

1) Algorithm Accuracy Comparison

Taking the signal of simulation case 2 as an example, a Gaussian white noise with a SNR of 10 dB is added, and the LFO oscillation parameters of the signal are identified using WT, HHT, Prony, and the proposed AD method. The results are shown in Figs. 16 and 17. It can be seen that the HHT and AD methods are more accurate in identifying the parameters of LFO indicators, while the WT and Prony methods are more sensitive to noise.

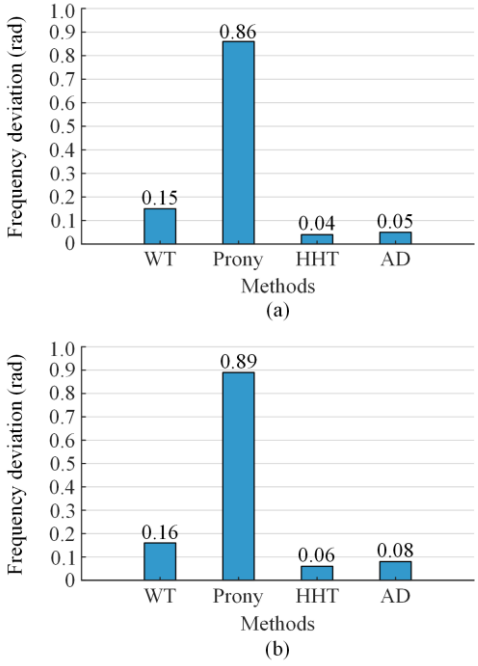

Fig. 16. Frequency deviation comparison of each method. (a) LFO mode 1 (53.8 Hz). (b) LFO mode 2 (46.2 Hz).

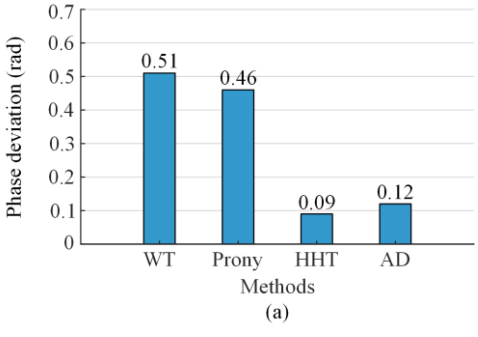

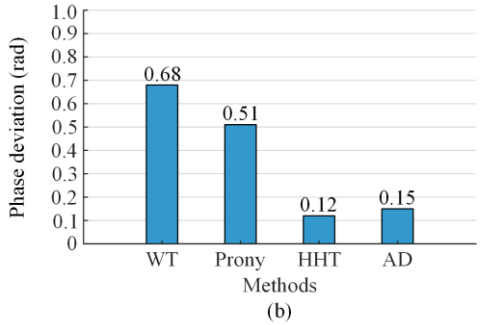

Fig. 17. Phase deviation comparison of each method. (a) LFO mode 1 (53.8 Hz). (b) LFO mode 2 (46.2 Hz).

2) Algorithm Speed Comparison

For practical implementation in an online monitoring system, computational speed is a critical performance metric, as even short-term LFOs can result in significant operational losses. Therefore, the proposed algorithm must be capable of rapidly identifying LFO modal information to meet the real-time requirements of such systems. Cases 1 and 2 are used to evaluate computational performance. The execution time of each algorithm is recorded, and the corresponding time consumption curves are plotted, as shown in Figs. 18 and 19 for case 1 and 2, respectively.

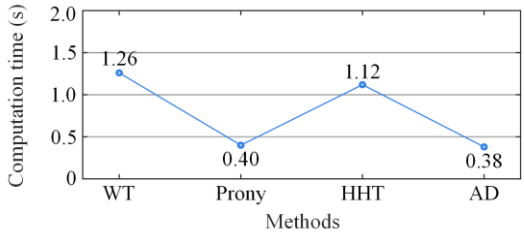

Fig. 18. Comparison of time consumption of various algorithms in simulation case 1.

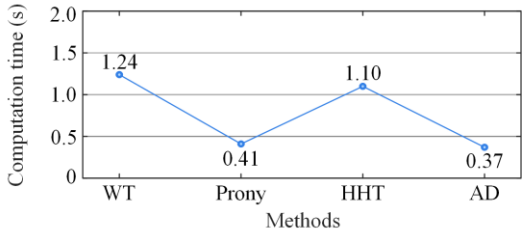

Fig. 19. Comparison of time consumption of various algorithms in simulation case 2.

Based on the above analysis, it can be observed that the Prony and AD methods require relatively low computational time, making them more suitable for real-time applications. In contrast, the WT and HHT methods involve higher computational complexity and longer processing times, thereby limiting their applicability in real-time LFO monitoring scenarios.

3) Algorithm Noise Resistance Comparison

Noise resistance of an algorithm reflects its ability to maintain accurate performance under noisy conditions. Random fluctuations caused by system load variations, as well as noise introduced during data acquisition and transmission, can significantly degrade signal quality. Therefore, the noise robustness of the detection algorithm is critically important. To evaluate and compare the noise resistance and robustness of each method, the simulation signal from case 2 is used with Gaussian white noise of varying SNRs of 5 dB, 10 dB, 15 dB, 20 dB, 25 dB, and 30 dB added. The four different algorithms are then applied to perform LFO identification under each noise level, and the corresponding results are illustrated in Fig. 20.

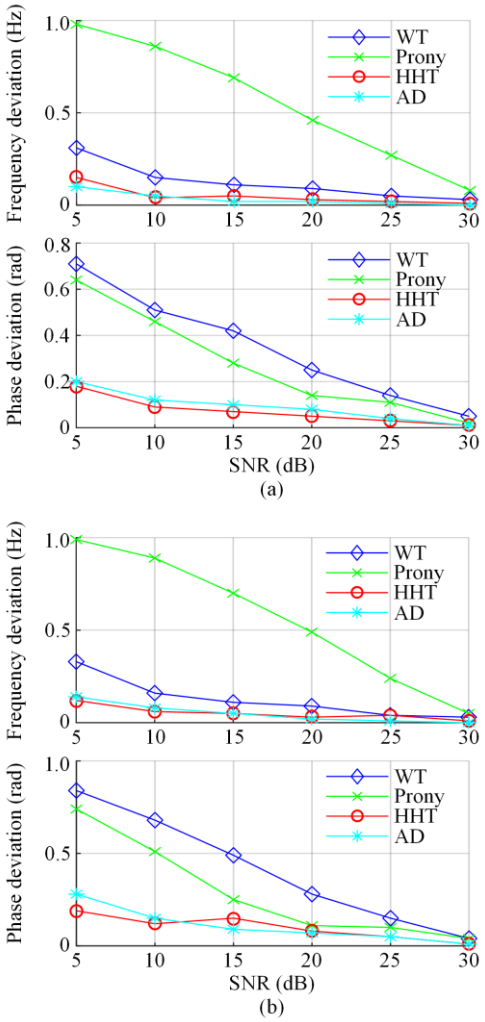

Fig. 20. Comparison of noise resistance performance of various algorithms. (a) LFO mode 1 (53.8 Hz). (b) LFO mode 2 (46.2 Hz).

As shown in Fig. 20, the identification errors of various parameters exhibit an overall decreasing trend as the level of Gaussian white noise decreases. Among the four algorithms, the Prony method is most sensitive to noise interference. At a high SNR of 30 dB, its performance is comparable to those of the other algorithms; however, as the noise level increases (i.e., SNR decreases), the parameter identification errors of the Prony method increase rapidly. In contrast, the HHT and AD algorithms demonstrate greater robustness to noise. Even under low SNR conditions, their identification errors remain relatively stable and consistently low, indicating strong noise resistance and reliable performance in practical applications.

C. The Influence of Different Time Window Lengths

In order to verify the performance of the proposed algorithm under different time windows, taking the signal $u(t)$ of case 1 as an example, Gaussian white noise with a SNR of 10 dB is added, and the time windows are selected as 0.3 s, 0.5 s, and 1 s respectively to verify the performance of the proposed algorithm. The results are shown in Table V.

TABLE V
PERFORMANCE OF THE ALGORITHM UNDER DIFFERENT TIME WINDOW LENGTHS

The time window duration (s)	Calculated frequency value (Hz)	Frequency error (%)	Calculated phase value (Hz)	Phase error (%)	Computation time (s)
1	57.25	0.03	–2.80	1.45	0.81
0.5	57.16	1.20	–2.56	7.25	0.40
0.3	56.98	4.40	–2.36	14.49	0.27

As seen from Table V, although shortening the time window can reduce the delay in real-time detection, is also decreases the calculation accuracy, as shorter time windows are more sensitive to transient interference and Gaussian noise.

D. Measured Data Verification

To evaluate the practical performance of the proposed method in real-world TPSSs, as well as its real-time capability when processing large-scale data, this section analyzes measured LFO data obtained from real substations and multiple types of electric trains.

1) Measured Data Case 1: Urumqi Railway Hub

In the first test case, LFO data recorded at the Urumqi railway hub in China is selected for validation. The voltage and current waveforms are captured by a monitoring system during an oscillation event lasting 160 s, as shown in Fig. 21.

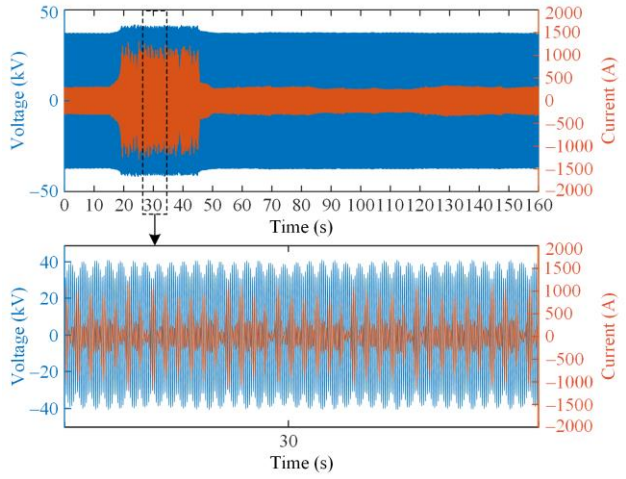

Fig. 21. Voltage and current waveforms of measured data case 1.

From the measured waveforms, it can be observed that continuous oscillations in both voltage and current signals began around 20 s, persisted for approximately 25 s, and then returned to a stable state at approximately 45 s. The algorithm recognizes that the LFO occurs in the time period of 19–45 s, and the corresponding results are shown in Figs. 22 and 23.

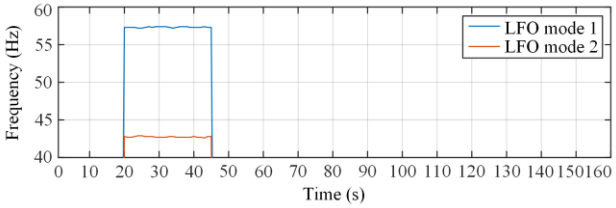

Fig. 22. LFO frequency identification results of measured data case 1.

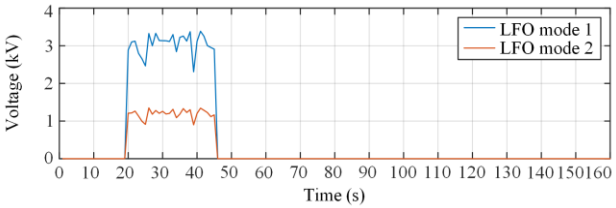

Fig. 23. LFO amplitude identification results of measured data case 1.

From the above results, during the period from 20 s to 45 s, the voltage signal exhibits continuous LFOs. The average frequency of the dominant oscillatory component is 57.3 Hz, and the maximum RMS value of the oscillating voltage reached 3.39 kV at 41 s, which aligns well with the characteristics observed in the original waveform data. Regarding real-time performance, the proposed algorithm processes the entire 160-second voltage waveform in only 14.8 s. Notably, the majority of the computation time is concentrated in the parameter identification stage during the oscillation interval.

2) Measured Data Case 2: CRH5G Train

The measured LFO data of CRH5G train is selected for verification in the second test case. The 160-second voltage and current waveform data collected by the monitoring equipment are shown in Fig. 24. From the measured waveform, it can be seen that the voltage and current waveforms of the CRH5G train oscillate violently from about 60 s, and the waveforms gradually stabilize from about 140 s.

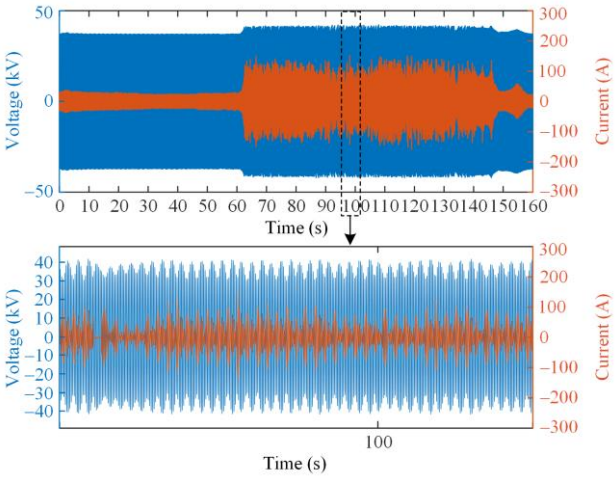

Fig. 24. Voltage and current waveforms of measured data case 2.

The detection results are shown in Figs. 25 and 26, indicating that the LFO occurs in the time period of 63–147 s and 154–156 s.

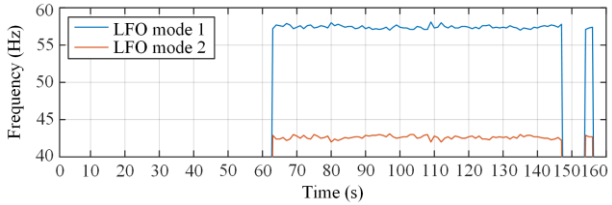

Fig. 25. LFO frequency identification results of measured data case 2.

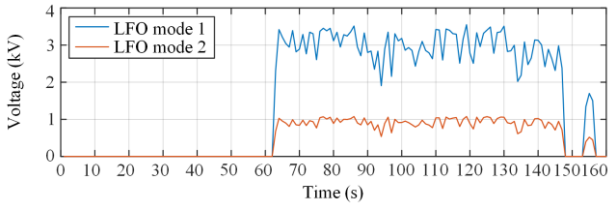

Fig. 26. LFO amplitude identification results of measured data case 2.

From the above results, during the period of 63–147 s, the voltage experiences continuous LFO, the average frequency of the dominant oscillation mode is 57.2 Hz, and the maximum effective value of the oscillating voltage reaches 3.55 kV (occurring at 119 s), which is consistent with the results reflected by the original waveform data. In terms of the real-time performance of the algorithm, for the above 160-second waveform data, the algorithm runtime is only 48.6 s.

3) Measured Data Case 3: CR200J Train

In the third test case, the measured LFO data of the CR200J locomotive is selected for verification. The 160-second voltage and current waveform data collected by the monitoring equipment are shown in Fig. 27. From the measured waveform, it is apparent that the voltage of the CR200J train oscillates violently at 40 s, but its current waveform remains largely unchanged. This behavior is likely due to the oscillations of other locomotives on the same feeder or other feeders on the same bus, forcing the CR200J locomotive to oscillate. The voltage waveform is gradually stabilized at about 105 s.

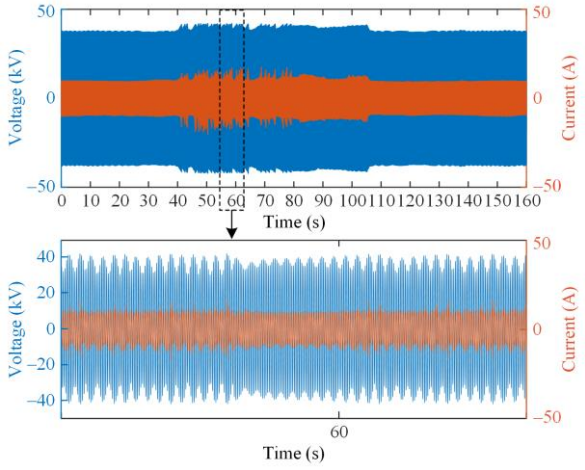

Fig. 27. Voltage and current waveforms of measured data case 3.

The detection results are shown in Figs. 28 and 29, indicating that the LFO occurs in the time period of 41–44 s, 46–65 s, and 68–106 s.

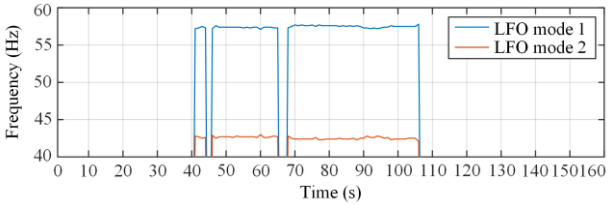

Fig. 28. LFO frequency identification results of measured data case 3.

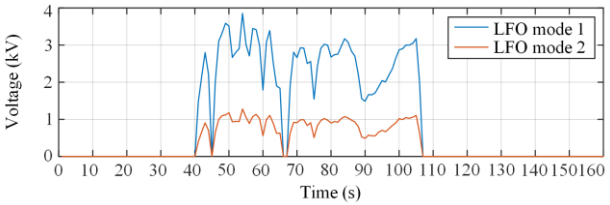

Fig. 29. LFO amplitude identification results of measured data case 3.

From the above results, during the period of 41 s to 106 s, the voltage experiences continuous LFO, the average frequency of the dominant oscillation component is 57.4 Hz, and the maximum oscillating voltage reaches 3.86 kV (occurring at 54 s), which is consistent with the results from the original waveform data. In terms of the real-time performance of the algorithm, for the above 160-second waveform data, the algorithm runtime is only 35.8 s.

According to Eq. (12), the waveform similarities between the reconstructed and original signal of the three measured data are shown in Table VI.

TABLE VI
THE WAVEFORM SIMILARITY BETWEEN THE RECONSTRUCTED AND ORIGINAL SIGNAL

Type	Urumqi hub	CRH5G train	CR200J train
Similarity (%)	99.88	99.92	99.92

The three measured data cases presented above demonstrate that the proposed method can not only rapidly identify the start and end times of LFO disturbances in practical data but also accurately extract their key parameters. Considering additional factors such as data storage and communication delays, the proposed algorithm significantly enhances the speed of LFO detection while maintaining high accuracy. These results demonstrate that the algorithm fully satisfies the requirements for real-time LFO monitoring in practical systems. Consequently, the proposed method shows strong potential for deployment in real-world online monitoring applications for LFOs in TPSSs.

IV. CONCLUSION

To address the need for rapid identification of LFO parameters in TPSSs, this paper proposes a real-time detection algorithm based on sparse representation. The approach begins by applying a low-pass filter to the traction

network voltage signal to suppress high-frequency noise, followed by real-time monitoring of low-frequency energy distribution using the FFT. When the amplitude within the target frequency band exceeds a predefined threshold, the parameter identification module is activated. The frequency domain is then re-discretized around the dominant low-frequency components identified via FFT, and an over-complete atomic dictionary tailored to LFO signal characteristics is constructed. Finally, the MP algorithm is employed to extract the LFO parameters, including oscillation frequency, amplitude, and phase, with high accuracy and efficiency.

Through extensive simulations involving complex disturbance signals and analysis of field-measured data, the proposed method has demonstrated its ability to rapidly and accurately detect LFOs in TPSSs. Compared to traditional MP-based algorithms, it significantly reduces the size of the atomic dictionary and lowers computational complexity, while maintaining strong robustness to noise and good generalization capability. These results confirm the superior performance of the proposed algorithm in real-time LFO monitoring applications.

Future research will focus on further improving computational efficiency for large-scale real-time deployment, as well as extending the algorithm's applicability to other types of power systems.

ACKNOWLEDGMENT

Not applicable.

AUTHORS' CONTRIBUTIONS

Jun Zhu: algorithm debugging and simulation data & measured data analysis. Zhaoyang Li: review writing and text editing. Yu Xie: assisted in obtaining field data. Haitao Hu: project administration, resources, and funding acquisition. All authors read and approved the final manuscript.

FUNDING

This work is supported by the National Natural Science Foundation of China (No. 52472420) and the Fundamental Research Funds for the Central Universities (No. 2682024CX081).

AVAILABILITY OF DATA AND MATERIALS

Not applicable.

DECLARATIONS

Competing interests: The authors declare that they have no known competing financial interests or personal relationships that could have appeared to influence the work reported in this article.

AUTHORS' INFORMATION

Jun Zhu received the B.S. degree in electrical engineering from the Jinling Institute of Technology, Nanjing, China, in 2017. He is currently pursuing the Ph.D. degree in electrical engineering with Southwest Jiaotong University, Chengdu, China. His current research interests include the energy consumption and power quality monitoring of electrified railway.

Zhaoyang Li received the B.S. and Ph.D. degrees in electrical engineering from Southwest Jiaotong University, Chengdu, China, in 2014 and 2020, respectively.,He is currently an assistant professor with Southwest Jiaotong University. His research interests include measurement, analysis and control of power quality, and harmonics in power systems.

Yu Xie received the B.E. degree in electrical engineering from Southwest Petroleum University, Chengdu, China, in 2024. He is currently working toward the M.S. degree in electrical engineering with Southwest Jiaotong University, Chengdu. His current research interests focus on power quality monitoring, including the development of advanced detection algorithms, data-driven anomaly diagnosis, and the implementation of real-time monitoring systems for modern power grids.

Haitao Hu received the B.S. degree in electrical engineering from Zhengzhou University, Zhengzhou, China, in 2010, and the Ph.D. degree in electrical engineering from Southwest Jiaotong University, Chengdu, China, in 2014. From 2013 to 2014, he was a visiting doctoral scholar with the University of Alberta, Edmonton, AB, Canada. He is currently a professor with the College of Electrical Engineering, Southwest Jiaotong University. His current research interests include power quality and harmonics of the electric traction system.

REFERENCES

[1] H. Hu, Y. Zhou, and X. Li *et al*., "Low-frequency oscillation in electric railway depot: a comprehensive review," *IEEE Transactions on Power Electronics*, vol. 36, no. 1, pp. 295-314, Jan. 2021.

[2] H. Hu, Y. Shao, and L. Tang *et al*., "Overview of harmonic and resonance in railway electrification systems," *IEEE Transactions on Industry Applications*, vol. 54, no. 5, pp. 5227-5245, Sept. 2018.

[3] H. Hu, H. Tao, and F. Blaabjerg *et al.*, "Train-network interactions and stability evaluation in high-speed railways—part I: phenomena and modelling," *IEEE Transactions on Power Electronics*, vol. 33, no. 6, pp. 4627-4642, Jun. 2018.

[4] H. Hu, H. Tao, and X. Wang *et al*., "Train-network interactions and stability evaluation in high-speed railways—part II: influential factors and verifications," *IEEE Transactions on Power Electronics*, vol. 33, no. 6, pp. 4643-4659, Jun. 2018.

[5] Y. Liao, Z. Liu, and H. Zhang *et al.*, "Low-frequency stability analysis of single-phase system with *dq*-frame

impedance approach—part I: impedance modeling and verification," *IEEE Transactions on Industry Applications*, vol. 54, no. 5, pp. 4999-5011, Sept. 2018.

[6] H. Wang, M. Wu, and J. Sun, "Analysis of low-frequency oscillation in electric railways based on small-signal modeling of vehicle-grid system in dq frame," *IEEE Transactions on Industry Applications*, vol. 30, no. 9, pp. 5318-5330, Sept. 2015.

[7] M. M. Steinar Danielsen, T. Toftevaag, and O. B. Fosso, "Constant power load characteristic's influence on the low-frequency interaction between advanced electrical rail vehicle and railway traction power supply with rotary converters," in *Modern Electric Traction 9th International Conference*, Warsaw, Poland, Sept. 2009, pp. 1-6.

[8] F. Zou, "Research on low-frequency oscillation problems of electrified railway vehicle network," M.S. thesis, Department of Electric Engineering, Beijing Jiaotong University, Beijing, China, 2024.

[9] J. Yu, "Research on online identification algorithm of abnormal electrical disturbance and broadband impedance in traction power supply system," M.S. thesis, Department of Electric Engineering, Southwest Jiaotong University, Chengdu, China, 2023.

[10] J. Jia, "Research on the electrical matching problem and monitoring algorithm of Sichuan-Tibet Railway," M.S. thesis, Department of Electric Engineering, Beijing Jiaotong University, Beijing, China, 2021.

[11] H. Zhang, J. Xiong, and X. Cai, "Power harmonic analysis based on high oversampling and windowed interpolation FFT," *Power Systems Protection and Control*, vol. 52, no. 5, pp. 105-115, Mar. 2024. (in Chinese)

[12] H. Wang, S. He, and S. Hu, "Research on fault identification and location method based on wavelet transform and TKEO," *Power Systems Protection and Control*, vol. 53, no. 14, pp. 177-187, Jul. 2025. (in Chinese)

[13] M. Ruan, Y. Cheng, and T. Zhang *et al.*, "Improved Prony method for high-frequency-resolution harmonic and interharmonic analysis," in *2019 IEEE 2nd International Conference on Electronics Technology (ICET)*, Chengdu, China, May 2019, pp. 585-589.

[14] J. Tian, J. Zhao, and G. Zeng *et al.*, "Data-driven modeling of modular multilevel converters based on HHT and CNN-LSTM-AM neural network," *IEEE Transactions on Industrial Electronics*, vol. 72, no. 9, pp. 8725-8735, Sept. 2025.

[15] D. L. Donoho and X. Huo, "Uncertainty principles and ideal atomic decomposition," *IEEE Transactions on Information Theory*, vol. 47, no. 7, pp. 2845-2862, Nov. 2001.

[16] F. Zhou, F. Liu, and R. Wang *et al*., "Identification of electrical coupling anomalies in electrified railways," *Proceedings of the CSEE*, vol. 41, no. 23, pp. 7937-7950, Jun. 2021. (in Chinese)

[17] F. Zhou, T. Yang, and F. Liu *et al.*, "Electrical anomaly identification of vehicle-grid coupling system based on wavelet packet decomposition and extreme gradient boosting," *Journal of the China Railway Society*, vol. 44, no. 12, pp. 58-68, Dec. 2024. (in Chinese)

[18] J. Yu, H. Hu, and H. Tao, "Online identification and evaluation algorithm of abnormal disturbance in traction power supply system," *Electric Power Automation Equipment*, vol. 43, no. 8, pp. 217-224, Dec. 2023. (in Chinese)

[19] S. Mallat and Z. Zhang, "Matching pursuits with time-frequency dictionaries," *IEEE Transaction on Signal Process,* vol. 41, no. 12, pp. 3397-3415, Dec. 1993.

[20] Y. Zhang, Q. Gong, and X. Li *et al.*, "Application of atomic decomposition method based on PSO in interharmonic analysis," *Power System Protection and Control*, vol. 41, no. 15, pp. 41-48, Jul. 2013. (in Chinese).

[21] Y. Li, Z. Teng, and Z. Ji *et al*., "Harmonic and interharmonic detection method based on improved ICA-OMP optimized atomic decomposition," *Chinese Journal of Scientific Instrument*, vol. 43, no. 7, pp. 247-256, Jun. 2022. (in Chinese)

[22] M. S. Manikandan, S. R. Samantaray, and I. Kamwa, "Detection and classification of power quality disturbances using sparse signal decomposition on hybrid dictionaries," *IEEE Transactions on Instrumentation and Measurement*, vol. 64, no. 1, pp. 27-38, Jan. 2015.

[23] L. Lovisolo, E. A. B. da Silva, and M. A. M. Rodrigues *et al*., "Efficient coherent adaptive representations of monitored electric signals in power systems using damped sinusoids," *IEEE Transactions on Signal Processing*, vol. 53, no. 10, pp. 3831-3846, Oct. 2005.

[24] Z. Zheng, J. Xu, and M. Guo, "Online identification method of distribution line-to-ground parameters and grounding transition conductance during arc suppression," *Protection and Control of Modern Power Systems*, vol. 10, no. 4, pp. 103-115, Jul. 2025.

[25] Y. Wang, Y. Li, and Z. Qu *et al.*, "Power quality disturbance identification based on PSO-MP algorithm and RBF neural network," *Electrical Measurement and Instrumentation*, vol. 53, no. 13, pp. 54-58, Jul. 2016. (in Chinese)

[26] Z. Cui, N. Wang, and Q. Jia, "Parameter identification method of power quality composite disturbance based on hierarchical matching pursuit algorithm," *Electric Power Automation Equipment*, vol. 37, no. 3, pp. 153-159, Mar. 2017. (in Chinese)

[27] H. Li, C. Li, and Z Wang, "Application of direct decaying sine atom library decomposition method based on combined optimization of chaos and Pseudo-Newton method in low frequency oscillation analysis," *Proceedings of the CSEE*, vol. 38, no. 1, pp. 148-157, Aug. 2018. (in Chinese)

[28] X. Li and Q. Gong, "Review of dynamic characteristics analysis methods of low-frequency oscillation modes in power systems," *Shaanxi Electric Power*, vol. 41, no. 12, pp. 24-29, Dec. 2013. (in Chinese)

[29] B. Yang, Y. Zhou, and Y. Yan, *et al.* "A critical and comprehensive handbook for game theory applications on new power systems: structure, methodology, and challenges," *Protection and Control of Modern Power Systems.* vol. 10, no. 5, pp. 1-27, Sept. 2025.

[30] H. Wang, "Research on electrical low-frequency oscillation of electrified railway network," Ph.D. dissertation, Department of Electric Engineering, Beijing Jiaotong University, Beijing, China, 2015.

[31] S. He, K. Li, and D. Cai *et al.*, "Optimal resolution extraction of power quality disturbance data features," *Proceedings of the CSEE*, vol. 38, no. 21, pp. 6223-6232, 6484, Jul. 2018. (in Chinese)